Effect of Different Nanoparticles on Thermal, Mechanical and Dynamic Mechanical Properties of Hydrogenated Nitrile Butadiene Rubber Nanocomposites

Anusuya Choudhury,[1] Anil K. Bhowmick,[1] Christopher Ong[2]

[1]*Rubber Technology Centre, Indian Institute of Technology, Kharagpur, Kharagpur 721302, India*
[2]*LANXESS Deutschland GmbH, Dormagen 41538, Germany*

Received 28 June 2008; accepted 17 June 2009
DOI 10.1002/app.30985
Published online 4 January 2010 in Wiley InterScience (www.interscience.wiley.com).

ABSTRACT: Organically modified and unmodified montmorillonite clays (Cloisite NA, Cloisite 30B and Cloisite 15A), sepiolite (Pangel B20) and nanosilica (Aerosil 300) were incorporated into hydrogenated nitrile rubber (HNBR) matrix by solution process in order to study the effect of these nanofillers on thermal, mechanical and dynamic mechanical properties of HNBR. It was found that on addition of only 4 phr of nanofiller to neat HNBR, the temperature at which maximum degradation took place (T_{max}) increased by 4 to 16°C, while the modulus at 100% elongation and the tensile strength were enhanced by almost 40–60% and 100–300% respectively, depending upon nature of the nanofiller. It was further observed that T_{max} was the highest in the case of nanosilica-based nanocomposite with 4 phr of filler loading. The increment of storage modulus was highest for sepiolite-HNBR and Cloisite 30B-HNBR nanocomposites at 25°C, while the modulus at 100% elongation was found maximum for sepiolite-HNBR nanocomposite at the same loading. A similar trend was observed in the case of another grade of HNBR having similar ACN content, but different diene level. The results were explained by x-ray diffraction, transmission electron microscopy, and atomic force microscopy studies. The above results were further explained with the help of thermodynamics. Effect of different filler loadings (2, 4, 6, 8, and 16 phr) on the properties of HNBR nanocomposites was further investigated. Both thermal as well as mechanical properties were found to be highest at 8 phr of filler loading. © 2010 Wiley Periodicals, Inc. J Appl Polym Sci 116: 1428–1441, 2010

Key words: hydrogenated nitrile rubber; nanofillers; thermal properties; mechanical properties; dynamic mechanical properties

INTRODUCTION

Hydrogenated nitrile rubber (HNBR) has been developed to improve thermal stability of nitrile butadiene rubber (NBR).[1–3] During hydrogenation of NBR, a small number of double bonds and all the cyano groups are kept unhydrogenated for subsequent sulfur vulcanization and oil resistance. This elastomer is known for its physical strength and retention of properties after long term exposure to heat, oil, and chemicals. Because of these unique properties, HNBR is widely used in automotive, industrial and assorted performance demanding applications, where still higher heat and oil resistant properties are required. Addition of small amount of nanofillers may improve the properties of this rubber further.

In the polymer industry, polymer-filler nanocomposites are a promising class of material that offers the possibility of developing new hybrid materials with desired set of properties.[4–9] Polymer nanocomposites have attracted great attention since Toyota group showed a considerable enhancement of properties of nylon by incorporating layered silicates. These show better thermal, mechanical, barrier and other properties because of excellent dispersion of filler and stronger interfacial force between the nanometer sized filler and a polymer, than conventional polymer-filler composites.[10–18]

Among the conventional nanofillers, clay is extensively used in the polymer industry. Depending on the nature of nanoclays, these can be divided into different types: 1) Smectite/montmorillonite Group, 2) Kaolinite Group, 3) Mica and 4) Sepiolite. On the other hand, silica is known as reinforcing filler having the particle dimension ranging from 10 to 20 nm.

Numerous research work has been done based on montmorillonite clay using a variety of polymers.[19–30] However, very little work has been done on sepiolite and silica based polymer

Correspondence to: A. K. Bhowmick (anilkb@rtc.iitkgp.ernet.in).
Contract grant sponsor: LANXESS.

nanocomposites.[22,31–33] In this study, we have used silica nanofiller, organically modified, and unmodified montmorillonite clays and organically modified sepiolite, to improve thermal stability, mechanical and dynamic mechanical properties of HNBR.

Montmorillonite is a derivative of pyrophyllite and has a 2 : 1 layer structure consisting of two fused silica tetrahedral sheets sandwiching an octahedral sheets of alumina [Fig. 1(a)]. It has layer charges due to isomorphic substitution, which occurs when some atoms in the crystal structure are replaced with some other atoms with different valance without any change of the crystal structure. As a result, montmorillonite contains excess negative charge in its structure and can adsorb cations with an electric quantity equivalent to that of montmorillonite. Hydrated cations enter the interlayer region which then leads to an increase in the distance between the adjacent layers. Natural Na-montmorillonite (here Cloisite NA) is hydrophilic and is not compatible with most organic polymers. However, sodium cations in the interlayer space of montmorillonite can be exchanged with organic cations to yield organophilic montmorillonite.

Sepiolite is a crystalline hydrated magnesium silicate with unique three dimensional structures and has a fibrous morphology. Like montmorillonite, sepiolite is a 2 : 1 phyllosilicate, where one octahedral sheet is sandwiched between two tetrahedral sheets. The tetrahedral sheets are extended to a considerable distance in the "a" and "b" directions (Fig. 2). However, at periodic intervals along the b-axis, the tetrahedral sheets invert and hence sepiolite is also called an "inverted ribbon." This generates a microporous structure with a large surface area, which is responsible for its adsorption properties and derived applications. Its chemical formula for a half unit cell is given as $[(Si_{12})(Mg_8)O_{30}(OH)_4(OH_2)_4 8H_2O]$. It contains fine micropore channels of dimension 0.37×0.16 nm^2 running parallel to the length of the fiber. The parallel piped fibers are bundled together along the c-axis. Thus, micro channels exist along the c-axis and contain free water (zeolite water) molecules attached to the edge of the octahedral layer. Sepiolite, because of its fibrous morphology, high aspect ratio and presence of high density of silanol group, is expected to have a good interaction with the polar groups of the rubber chain.

Silica particles are commonly used to improve tear strength, reduce heat build up, lower shrinkage on curing and decrease thermal expansion coefficient and meet specific mechanical properties. The improvement of properties is mainly due to the creation of hydrogen bond between the hydroxyl groups on the nanosilica surface and soft segment of a rubber.

In the present work, various nanocomposites based on HNBR have been prepared and extensively characterized. The effects of different nanofillers on the thermal, mechanical, and dynamic mechanical properties of the elastomer have been investigated. The results have been explained by x-ray diffraction (XRD) and transmission electron microscopy, where interaction of different nanofillers with the elastomer and the subsequent dispersion of these fillers are evident. Finally, a thermodynamic interpretation of the results has been made.

EXPERIMENTAL

Materials

Therban C3467 (having acrylonitrile content = 34%, diene content = 5.5%, Mooney viscosity, $ML_{(1+4)}$ at 100°C = 68, specific gravity = 0.95) and Therban A3407 (having acrylonitrile content = 34%, diene content = 0.9%, Mooney viscosity, $ML_{(1+4)}$ at 100°C = 70 and specific gravity = 0.95) were obtained from Lanxess, Germany. The clays used in this study were Cloisite 30B (produced by ion exchange of a methyl tallow bis-2-hydroxy quaternary ion), Cloisite 15A [prepared by ion exchange of naturally occurring sodium with quaternary ammonium (dimethyl dihydrogenated tallow) ion], Cloisite NA (a natural clay containing no organic surfactant) and sepiolite, Pangel B20 (hydrous magnesium silicate having no substitution in its lattice structure and modified by quaternary ammonium salt) (Table I). These organically modified and unmodified montmorillonite clays (Cloisite NA, Cloisite 30B and Cloisite 15A) were purchased from Southern Clay Products, Gonzales, TX and sepiolite Pangel B20 was gifted by Tolsa S.A, Pque, Empres, Mercedes, Spain. Nanosilica used was Aerosil®300 from Degussa GmbH, Germany. Designation of these nanofillers is listed in Table I. The solvents used in this study were supplied by Merck Limited, Mumbai, India.

Preparation of rubber-clay nanocomposites

The rubber was first dissolved in chloroform (10% rubber solution w/v). The clay was dispersed in methyl ethyl ketone, by sonicating in an ultrasonicator for 30 min (1 g in 50 mL) at 25°C. The selection of solvent was done on the basis of knowledge from our previous work.[34] The clay dispersion was then poured into the prepared rubber solution and stirred for 3 h in a magnetic stirrer at room temperature followed by 30 min vigorous stirring with a mechanical stirrer to make a homogenous mixture. The solution was finally cast on a Petri dish to get a thin film. The solvent was allowed to evaporate at room temperature and the film was dried in a vacuum oven

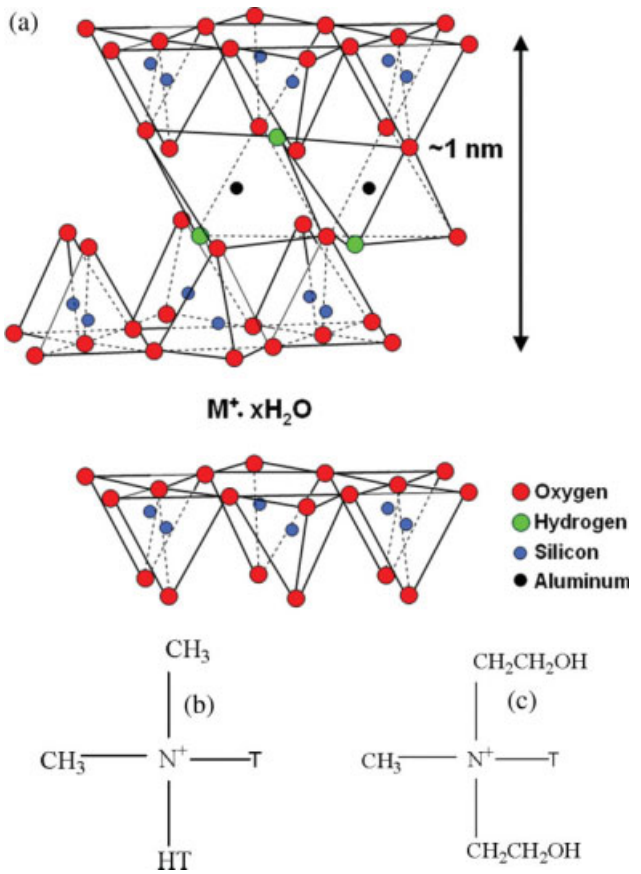

Figure 1 (a) Structure of natural montmorillonite, (b) surfactant present in 15A, and (c) surfactant present in 30B [T = tallow (~ 65% C18; 30% C16; ~ 5% C14, like stearic acid)]. [Color figure can be viewed in the online issue, which is available at www.interscience.wiley.com.]

at 50°C, till there was no weight variation. The designation of different grades of rubber and their nanocomposites is represented in Table II.

X-ray diffraction (XRD)

For the characterization of the nanocomposites, XRD studies were performed on a PHILIPS X-PERT PRO diffractometer in the range of 2–9°(2θ) using Cu target (λ = 0.154 nm). The d-spacing of the clay particles was calculated using the Bragg's law.

Transmission electron microscopy (TEM)

The samples for TEM analysis were prepared by ultracryomicrotomy with a Leica Ultracut UCT (Leica Microsystems GmbH, Vienna, Austria). Freshly sharpened glass knives with cutting edges of 45° were used to obtain cryosections of about 100 nm thickness at −90°C. The cryosections were collected individually in sucrose solution and directly supported on a copper grid of 300 mesh size. Transmission electron microscope (JEOL 2100, Japan) was operated at an accelerating voltage of 200 KV.

Thermogravimetric analysis

Thermogravimetric analysis was done using Perkin–Elmer Instrument, Diamond TG-DTA. The samples (3–5 mg) were heated from ambient temperature to 800°C in the furnace of the instrument under air atmosphere at 60 ml/min at a heating rate of 20°C/min. Analysis of the derivative thermogravimetric (DTG) curves was done and the onset temperature, weight loss at major degradation steps and the temperature corresponding to the maximum degradation in the derivative thermogram were recorded. The temperature at which maximum degradation took place is denoted as T_{max} and the corresponding onset temperature of degradation (5% degradation) is represented as T_i. The error in the measurement was ±1°C.

Mechanical properties

Tensile specimens were punched out from the cast sheets using ASTM Die-C. The tests were carried out as per the ASTM D 412-98 method in a Universal Testing Machine (Zwick/ Roell Z010) at a crosshead speed of 500 mm/min at 25°C. The average of three tests is reported here. The error was ±2% in the measurements of tensile strength and modulus, and ±5% for elongation at break (EAB).

Dynamic mechanical thermal analysis (DMTA)

The dynamic mechanical properties of the nanocomposites were measured by means of dynamic mechanical thermal analyzer, DMA Q500, using rectangular specimen having dimensions of 30 × 6.3 × 0.15 mm^3. The sample specimens were analyzed in tension mode in the temperature range of −70 to 70°C at a controlled heating rate of 2°C/min at a constant sinusoidal frequency of 1 Hz, at 0.01% strain amplitude. Storage modulus (E'), loss modulus (E''), and damping coefficient (loss factor, tan δ)

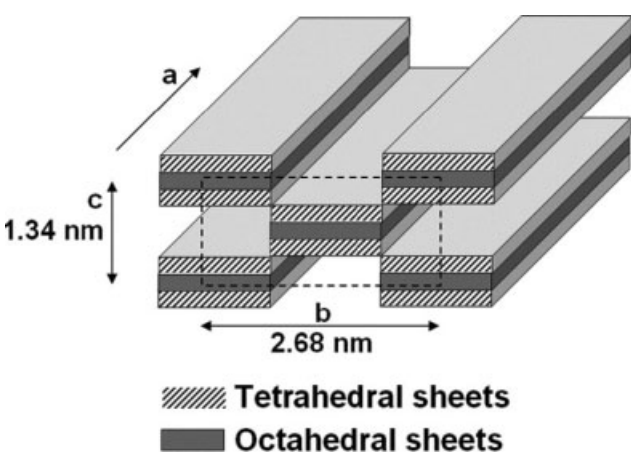

Figure 2 Structure of sepiolite.

TABLE I
Designation and Characteristics of Different Nanofillers

Nanofillers	Designation	Characteristics
Cloisite NA	NA	Surface area =750 m^2/g, layer thickness = 1 nm, aspect ratio = 50–200, initial particles consist of about 6000 platelets.
Cloisite 15A	15A	Substituted dimethyl dihydrogenated tallow montmorillonite, synthesized by ion-exchanging sodium montmorillonite clays. Cation-exchange capacity (CEC) = 1.25 mequiv/g with dimethyl dihydrogenated tallow (di-tallow) ammonium. The di-tallow is a mixture of dimethylammonium surfactants with various carbon chain lengths 65% of C18, 30% of C16, and 5% of C14. Moisture content = 2%
Cloisite 30B	30B	Substituted dimethyl dihydrogenated tallow (~ 65% C18; 30% C16; ~ 5% C14, like stearic acid) quaternary ammonium. Cation-exchange capacity (CEC) = 0.90 mequiv/g, Moisture content = 2%
Pangel B20	B20	Pangel B20 is an organophilic sepiolite, obtained from pristine sepiolite by means of specific physico-chemical purification, micronization and chemical modification processes. The micronization leads essentially to a disagglomeration of the bundles of microfibres. The hydrophilic surface of sepiolite was modified with surfactants in order to make it more compatible with low polarity polymers.
Aerosil®300	A300	Surface area = 300 (270–330) m^2/g, pH = 3.7–4.7, moisture content = 1.5% and SiO_2 content = 99.8%

were measured as a function of temperature for all the representative samples under identical conditions. The temperature corresponding to tan δ peak was taken as the glass transition temperature (T_g).

Fourier transform infra-red spectroscopy (FTIR)

Fourier transform infra-red spectroscopy (FTIR) study was done in a Perkin–Elmer FTIR Spectrometer 843, in the range 400–4000 cm^{-1} by casting a very thin film (~ 1% dispersion of the nanocomposite in chloroform). The specimen taken for the measurement had a thickness of 2 mm. An average of 32 scans is reported here.

RESULTS AND DISCUSSION

XRD studies

The X-ray diffractograms of different clays and their nanocomposites are shown in Figure 3(aI–dI). Figure 3(aI) represents traces for 30B and its nanocomposite at 4 phr loading. The clay, 30B, has a peak at an angle of 4.8°, corresponding to an interlayer distance of 1.97 nm, whereas the nanocomposite shows no such peak. This indicates a complete breakdown of the layer structure of the clay, leading to exfoliation. It is interesting to note that the two organically modified montmorillonite clays (30B and 15A) behave differently in HNBR. As can be seen from Figure 3(bI), 15A shows one sharp peak at 2.7°, corresponding to intergallery d-spacing of 3.26 nm and one small hump at 7° ($d \approx 1.26$ nm), while its nanocomposite has one small peak at 2.1° ($d = 4.27$ nm) and another one at 4.5° ($d = 1.98$ nm). Such a shift in the peaks towards lower 2θ value indicates that the rubber chains enter the clay layers, expanding the clay gallery spacing. However, as there is a small peak, it can be assumed that the clay layers do not exfoliate completely unlike 30B. The reason is explained in detail in the next section (TEM studies). The incorporation of tallow quaternary ammonium ions actually expands the gallery distance of 30B and 15A, which is further increased by HNBR.

TABLE II
Composition of HNBR-Filler Nanocomposites and their Designation

Composition	Designation
Therban C3467	S1
Therban C3467 + 2phr Pangel B20	S1-B20-2
Therban C3467 + 4phr Pangel B20	S1-B20-4
Therban C3467 + 6phr Pangel B20	S1-B20-6
Therban C3467 + 8phr Pangel B20	S1-B20-8
Therban C3467 + 16phr Pangel B20	S1-B20-16
Therban C3467 + 4phr Aerosil®300	S1-A300-4
Therban C3467 + 8phr Aerosil®300	S1-A300-8
Therban C3467 + 16phr Aerosil®300	S1-A300-16
Therban C3467 + 4 phr Closite 30B	S1-30B-4
Therban C3467 + 8 phr Closite 30B	S1-30B-8
Therban C3467 + 16 phr Closite 30B	S1-30B-16
Therban C3467 + 4 phr Closite 15A	S1-15A-4
Therban C3467 + 4 phr Closite NA	S1-NA-4
Therban A3407	S3
Therban A3407 + 4phr Pangel B20	S3-B20-4
Therban A3407 + 4phr Closite 30B	S3-30B-4
Theban A3407 + 4phr Closite 15A	S3-15A-4
Therban A3407 + 4phr Closite NA	S3-NA-4
Therban A3407 + 4phr Aerosil®300	S3-A300-4

However, exfoliation or intercalation is guided by the interaction of polymer chains with tallow amine and clay. It has been shown in the later section that there is favorable interaction in the case of S1-30B-4. In the case of NA, on the other hand, a 001 peak at $2\theta = 7.2^\circ$ corresponding to the interlayer spacing of 1.22 nm is observed [Fig. 3(cI)]. Surprisingly, the nanocomposite, i.e., S1-NA-4, has a peak at $2\theta = 5.2^\circ$ (a shift of 2°) corresponding to a gallery gap of 1.60 nm. This gallery gap is lower than those of 30B (1.97 nm) and 15A (3.26 nm). Sadhu and Bhowmick[15] in their work have reported that polybutadiene chains, being linear, can enter easily into the small gallery spacing of the unmodified NA and thus expands the clay layers. On the other hand, NBR, being bulky in nature cannot enter into the small gallery space of pristine clay. The bulky nature of the acrylonitrile groups present in the rubber can be better understood from the unperturbed or van der Waal chain dimensions. The average molecular weight per skeleton link for NBR is 107, while this value is 54 for polybutadine. This leads to a minimum interaction between the rubber (HNBR) and the pristine clay (NA) and consequently the clay layers do not generally exfoliate or intercalate within the polymer matrix. However, because of the high shear force during the preparation of the nanocomposites, some polymer molecules may enter into NA layers and expand the gallery gap slightly, as observed here.

The XRD traces for B20 and the corresponding nanocomposites demonstrate a completely different picture, as shown in Figure 3(dI). In the case of smectite clays, "exfoliation" refers to the separation of platelets followed by dispersion of those platelets throughout the polymer matrix. No such exfoliation is, however, observed in the case of B20, which are indeed fibrous in nature. Unlike smectite clays, here the fiber bundles or aggregates get separated in nanometer dimension which are then dispersed throughout the polymer matrix (discussed later). This is the reason why, the peak position of both the pristine clay as well as the clay in nanocomposite is the same in the XRD, i.e., $2\theta = 7.2^\circ$, corresponding to a gallery spacing of 1.21 nm.

TEM studies

TEM images of the nanocoposites are shown in Figure 3(aII–dII). From these images, the dispersion of the nanoparticles in the bulk of the matrix can easily be visualized. Figure 3(aII) confirms the well distribution of 30B particles within the matrix, indicating exfoliated morphology at 4 phr of filler loading. 30B, being an organically modified clay, has good compatibility with the organic polymer. Moreover, incorporation of the tallow quaternary ammonium ions expands the gallery gap between the clay layers. S1, having 34% ACN content, easily enters the clay gallery space and finally breaks the layer structure to form an exfoliated morphology. The observation is in line with the XRD results. However, TEM image of S1-15A-4 [Fig. 3(bII)] explains the presence of some tactoids, indicating intercalated morphology, which is also confirmed from the XRD results. 15A, having been modified by long chain amine groups, has a larger intergallery spacing (3.26 nm) than that of 30B (1.97 nm). Polymer chains can easily enter the intergallery space and the large spacing can facilitate their accommodation within the layers, thus forming an intercalated morphology. However, inadequate interaction between the polymer chains and clay/tallow amine due to the difference in structure, as shown in Figure 1(b,c) prevents exfoliation. The TEM photograph of S1-NA-4 [Fig. 3(cII)] demonstrates that only a few polymer chains can actually enter the clay layers, and most of the clay particles remain stacked causing agglomeration. Proper dispersion of clay platelets cannot be achieved in S1-NA-4 mostly due to incompatibility of the hydrophobic polymer with hydrophilic clay particles. S1, having 34% acrylonitrile content, is bulky in nature (average molecular weight per skeleton link is 107 compared to 54 for polybutadiene), and cannot enter the small gallery spacing of the unmodified NA and thus agglomeration is observed. This is also in line with the XRD result. Figure 3(dII) reveals fiber or rod like clay particles distributed throughout the matrix for S1-B20-4 nanocomposite.

Thus, TEM photographs of different nanocomposites are in full agreement with the XRD results.

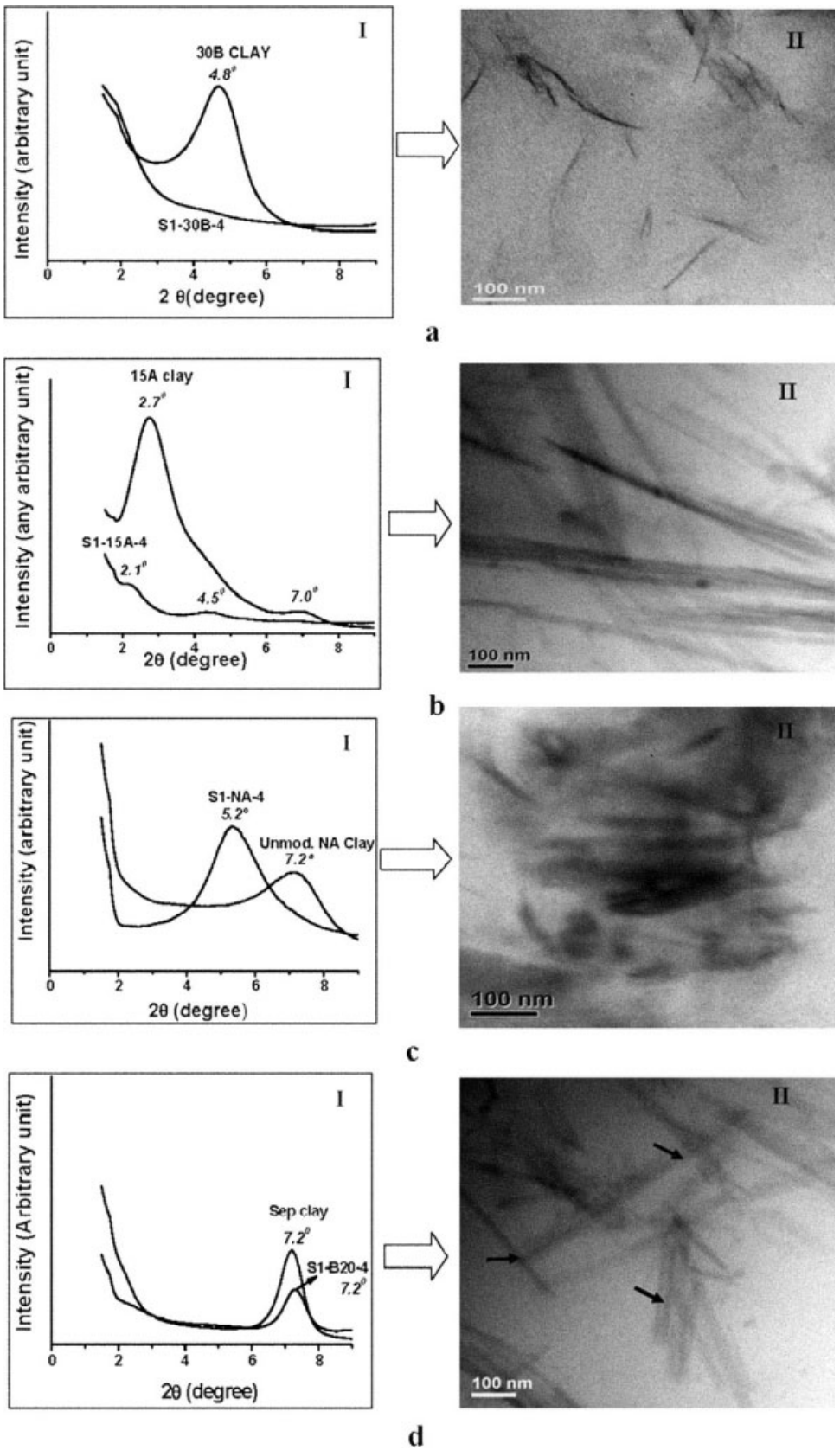

Figure 3 (I) XRD and (II) TEM photographs of (a) S1-30B-4, (b) S1-15A-4, (c) S1-NA-4, and (d) S1-B20-4.

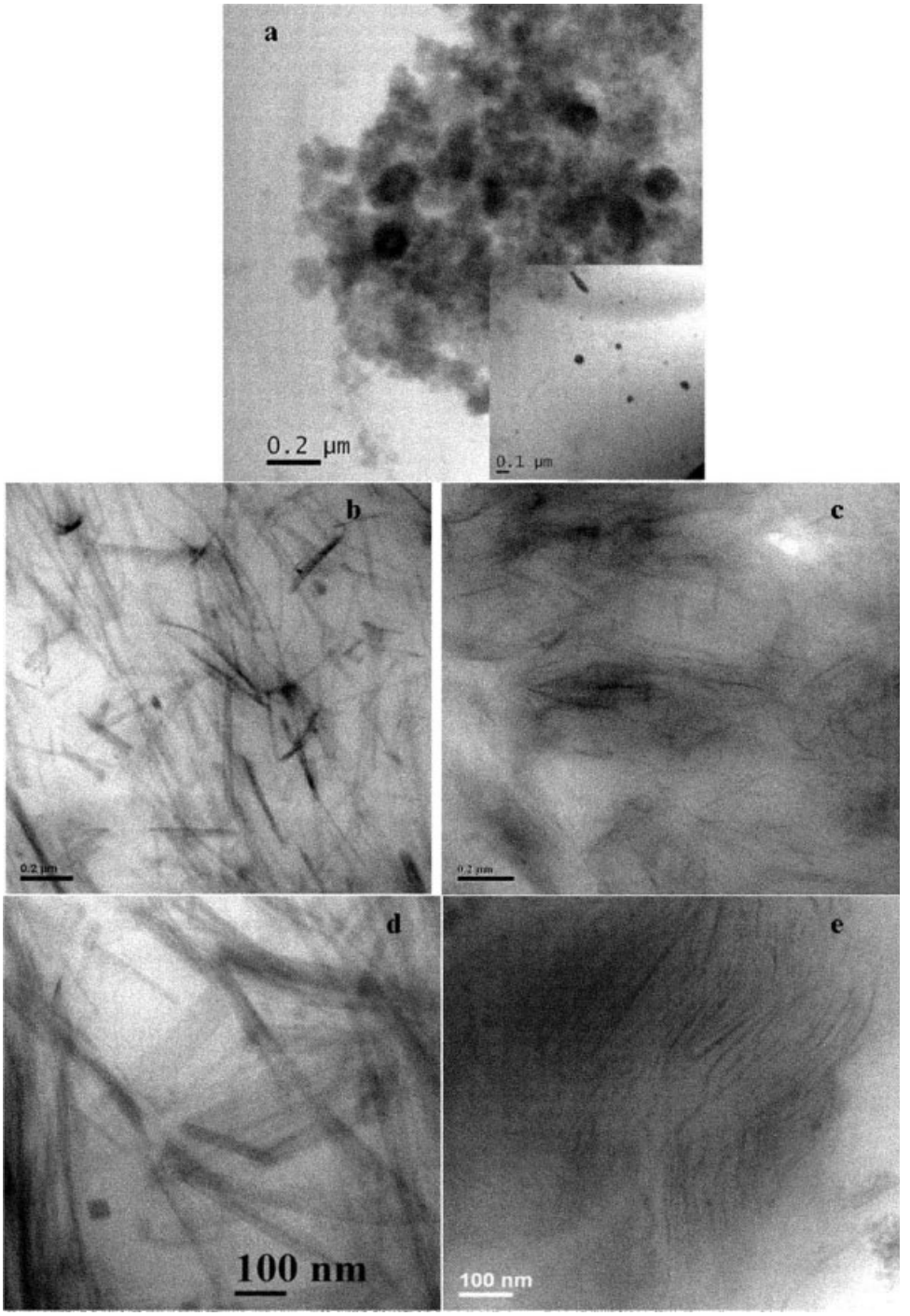

Figure 4 TEM photographs of (a) S1-A300-4, (b) S1-B20-8, (c) S1-30B-8, (d) S1-B20-16, and (e) S1-30B-16.

Figure 4(a) represents the TEM photograph of S1-A300-4. From the figure, it can be observed that some A300 particles in S1-A300-4 form network among themselves and thus get agglomerated, while few others remain unattached. A300 particles, because of having excess silanol group on their surface, have a strong tendency to form network among themselves and thus form agglomeration.

Figure 4(b–e) represents TEM photographs of S1-B20-8, S1-30B-8, S1-B20-16, and S1-30B-16. It is observed that higher the amount of nanofillers, more are the interacting sites available for the rubber matrix [Fig. 4(b,c)]. However, the nanofillers, having very high surface area, have a strong tendency to form agglomeration at further higher loading (S1-B20-16 and S1-30B-16), as observed in Figure 4(d,e).

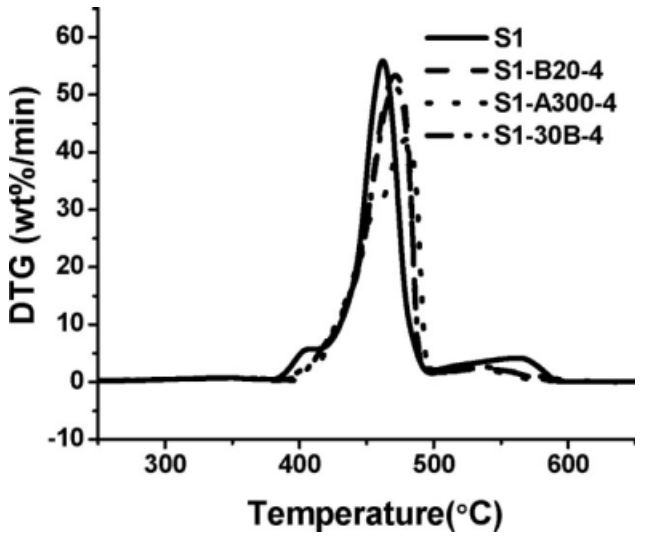

Figure 5 DTG vs. temperature curves for S1-filler nanocomposites with 4 phr of filler loading.

Thermal properties

Figure 5 shows the representative DTG thermograms of the unfilled and the nanofiller-filled HNBRs. As evident from the figure, there appears three different degradation temperatures for the neat rubber, one at 460°C and two very small humps at 403°C and 564°C respectively (Fig. 5). However, for the nanocomposites, DTG curves show single stage degradation with well defined initial and final degradation temperatures. The occurrence of small humps in the case of neat HNBR indicates formation of different stable intermediate products during oxidation. A similar phenomena had earlier been observed for NR and NBR degradation in N_2 and air.[3,35] Nanofillers form a protective layer on the surface of the matrix which, in turn, inhibits the oxidation process. As a result, these secondary peaks disappear on addition of the nanoparticles. The temperature corresponding to the major degradation (T_{max}), the onset of degradation (T_i), residue and maximum rate of degradation for all the samples are tabulated in Table III. T_i and T_{max} values increase respectively by 6°C and 12°C for S1-30B-4, 2°C and 6°C for S1-15A-4, 5°C and 12°C for S1-B20-4, and 6°C and 16°C for S1-A300-4. Thus, it is obvious from the above results that A300 provides excellent improvement in thermal property of the rubber. Such an improvement can be attributed due to the polar interactions between the filler and the rubber (evident from the shift of the IR peak of S1-A300-4 in Figure 9, discussed later) and also to the higher thermal stability of the inorganic filler. Moreover, A300 (silica) acts as a heat sink. Its specific heat capacity value is 700 J/(Kg.K), high enough to increase the thermal stability of the corresponding nanocomposites. Also, the thermal stability of A300 is higher than those of 30B and B20, as depicted in Figure 6. This explains why T_{max} of S1-A300-4 is higher than those of the other nanocomposites at 4 phr filler loading.

S1-30B-4 and S1-B20-4 also exhibit very high thermal stability. However, for S1-15A-4, there has been a marginal improvement in the thermal stability over the neat rubber. No such remarkable improvement in thermal property has been observed in the case of S1-NA-4 because of minimal interaction of the polymer with such clay as well as due to poor dispersion (explained by XRD studies and TEM photographs). 30B, on the contrary, is fully exfoliated (as observed from XRD and TEM photographs), and dispersed in nanometric levels throughout the matrix. As a consequence, it provides excellent thermal stability to the nanocomposite. 15A, however, bears

TABLE III
Effect of Nature of Filler and Filler Loading on Thermal Properties of HNBR-Filler Nanocomposites in Air at 20°C/min

Sl. no.	System	T_i (°C)	T_{max} (°C)	Residue (%)	DTG (wt %/min)
1	S1	439	460	0	54
2	S1- 30B-4	445	472	3	44
3	S1- 15A-4	441	466	3	51
4	S1- B20-4	444	472	3	50
5	S1- NA-4	437	464	3	52
6	S1- A300-4	445	476	3	42
7	S3	439	466	0	60
8	S3-30B-4	447	472	3	46
9	S3-15A-4	441	468	3	55
10	S3-B20-4	448	470	3	48
11	S3-NA-4	439	466	3	45
12	S3-A300-4	446	479	3	41
13	S1-B20-2	443	463	1	54
14	S1-B20-6	451	474	4	50
15	S1-B20-8	460	484	6	50
16	S1-B20-16	458	484	12	47

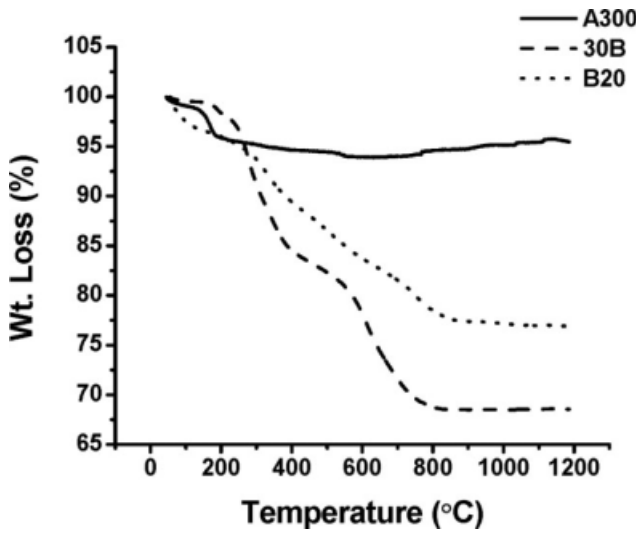

Figure 6 Weight loss vs. temperature curves of different nanofillers.

a large intergallery spacing (3.26 nm as obtained from the XRD studies) due to presence of long amine chains. It is known that a longer chain is always thermally less stable than a shorter one.[36] Also, it is a well known fact that exfoliated silicate layers provide better barrier property than that of an intercalated one.[36] 30B gets fully exfoliated within the matrix because of which it acts as strong barrier to gases such as oxygen and nitrogen, providing very good resistance to degradation for the nanocomposite. The intercalated morphology of 15A makes the barrier property of the corresponding nanocomposite inferior to that of S1-30B-4. On the other hand, because of fibrous/rod like nature, very high aspect ratio as well as good dispersion of filler throughout the bulk of the matrix (as clearly evident from TEM photographs), B20 improves the thermal properties of S1, similar to that of 30B.

The residues left after complete degradation of the nanocomposites are always found to be more than that of the neat rubber because of high thermal stability of the inorganic nanofiller, as represented in Table III.

Maximum rate of degradation for all the nanocomposites mentioned above are found to be lower than that of the neat rubber (Fig. 5). This is, due to fact that, nanofillers form a barrier over the surface of the rubber and hence, prevent diffusion of any gas either from the matrix to the environment or *vice versa*, thus decreasing the rate of degradation.

A similar trend is also observed in the case of S3, another grade of HNBR having 34% ACN content and 0.9% diene content, as shown in Table III (serial numbers 7 to 12). T_{max} is highest for S3-A300-4. In the case of S3-30B-4 and S3-B20-4, T_i increases respectively by 8 and 9°C, while T_{max} by 6°C and 4°C respectively when compared to those of the neat rubber. This indicates that both 30B and B20 have similar effects on the thermal stability of HNBR irrespective of the grade of rubber. However, for S3-NA-4, there has been no improvement in the thermal stability over the neat rubber, as represented in Table III (please refer to serial numbers 7 and 11 for comparison), because of poor rubber-clay interaction. The reason is same as explained above. The rate of degradation is also lower for all the nanocomposites over the neat rubber.

In order to understand the effect of filler loading on the thermal degradation of rubber-filler nanocomposites, S1-B20 nanocomposites were prepared at five different loadings, *viz*. 2, 4, 6, 8, and 16 phr. The values of T_i, T_{max} and % residues are tabulated in Table III (serial numbers 13, 4, 14–16). As expected,

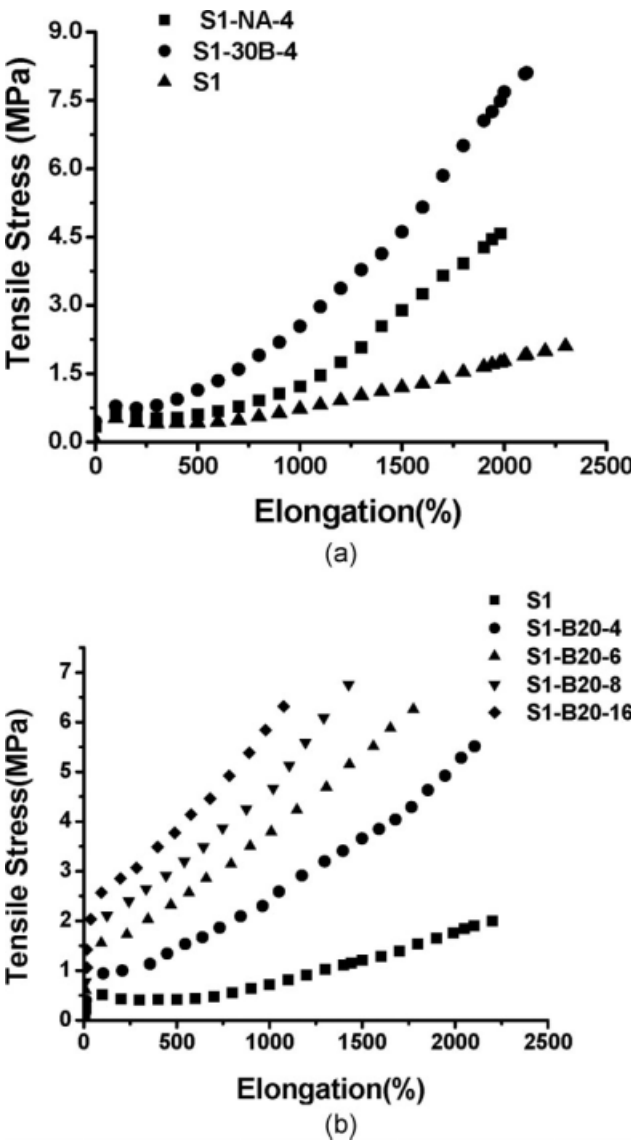

Figure 7 (a) Stress–strain curves of hydrogenated nitrile rubbers and its nanocomposites. (b) Stress–strain curves of hydrogenated nitrile rubbers with different filler loadings.

TABLE IV
Effect of Nature of Filler and Filler Loading on Mechanical Properties of HNBR-Filler Nanocomposites

Sl. no.	System	Modulus at 100 (MPa)	Young's modulus (kPa)	T.S. (MPa)	EAB (%)
1	S1	0.5 ± 0.02	2.0 ± 0.1	2.0 ± 0.1	>2300
2	S1-30B-4	0.7 ± 0.03	6.0 ± 0.2	8.0 ± 0.3	2100 ± 10
3	S1-15A-4	0.8 ± 0.05	6.0 ± 0.2	7.0 ± 0.3	1950 ± 5
4	S1-B20-4	1.1 ± 0.10	7.0 ± 0.3	6.0 ± 0.2	2000 ± 5
5	S1-NA-4	0.7 ± 0.03	3.0 ± 0.1	4.5 ± 0.3	2050 ± 5
6	S1-A300-4	0.6 ± 0.02	4.0 ± 0.2	5.5 ± 0.2	2150 ± 5
7	S3	0.6 ± 0.05	3.0 ± 0.1	3.0 ± 0.2	1600 ± 5
8	S3-30B-4	0.9 ± 0.10	5.0 ± 0.3	8.5 ± 0.4	2100 ± 5
9	S3-B20-4	1.5 ± 0.10	6.0 ± 0.4	6.5 ± 0.2	2000 ± 5

both T_i and T_{max} values increase with increase in filler loading and are highest for S1-B20-8. No further increase in thermal properties is observed, thereafter in the case of 16 phr of loading. This may be attributed to the fact that the rubber-filler interaction and dispersion are highest for 8 phr of loading [TEM photograph, Fig. 4(b)]. On the other hand, in the case of 16 phr, thermal properties decrease due to formation of agglomeration [Fig. 4(d)]. A similar trend is also observed for S1-30B and S1-A300 nanocomposites at different filler loadings (not shown here).

Mechanical properties

Stress–strain curves of some representative nanocomposites with various nanofillers at different filler loadings are represented in Figure 7(a,b). The results obtained from these curves are reported in Table IV. The modulus at 100% elongation and the tensile strength for S1 are 0.5 and 2.0 MPa, respectively. With the addition of 4 phr filler, these values increase by 40–60% and 280–300% respectively for both S1-30B-4 and S1-15A-4. A similar enhancement is obtained for the Young's modulus. For S1-B20-4, the modulus at 100% elongation increases by more than 100% and the tensile strength by 200%, and for S1-A300-4 these numbers are 20% and 175% respectively. However, these improvements are lowest for S1-NA-4 (Table IV). Thus, it is clear from Table IV that the modulus at 100% elongation is highest for S1-B20-4. B20, being fibrous in nature, has very high aspect ratio (ratio of particle length to width), which plays a major role in improving modulus at 100% elongation of the nanocomposites. Bokobza et al.[28] in their work reported that sepiolite improves the elastic modulus of poly(hydroxyethyl acrylate) by about three times than the neat polymer due to its high shape factor. On the other hand, the tensile strength is highest for S1-30B-4 followed by S1-15A-4 and lowest for S1-NA-4. Compatibility of 30B, 15A, and B20, the organically modified clays with organic polymer is much better than NA, which is unmodified montmorillonite clay. NA also has small intergallery spacing (only 1.22 nm as obtained from the XRD studies). Only few polymer chains can find their way into such a small gallery space, which results in poor polymer-filler interaction (as evident from the TEM photograph) and poor dispersion. 30B, on the other hand, is fully exfoliated (as observed from the XRD and TEM results), and dispersed into nanometric levels throughout the matrix. As a consequence, it provides excellent mechanical properties to the nanocomposite. From the TEM photograph, [Fig. 4(a)] it is clear that A300 has tendency to form agglomeration because of its large surface area and the presence of reactive sites in its structure. Such a tendency to form agglomeration reduces the mechanical properties of the S1-A300-4 to some extent. In spite of some agglomeration, the enhancement in tensile strength and modulus may be due to interaction between hydroxyl groups of silica with polar CN group of HNBR. A similar observation has been made for the dynamic mechanical properties of the nanocomposites, discussed in the next section.

A similar trend is also observed for another grade of HNBR (S3). The modulus at 100% elongation is highest for S3-B20-4, whereas the tensile strength is highest for S3-30B-4 (please refer to serial numbers 7–9 in Table IV) due to the same reason as explained earlier.

On incorporation of B20 at different filler loadings, the tensile strength increases up to 8 phr and thereafter falls at 16 phr loading, as shown in Figure 7(b). The modulus increases continuously with filler loading, while the elongation at break (EAB) goes on decreasing due to increased polymer-filler interaction and loading. Beyond 8 phr of filler loading, the strength, however, decreases, as the fillers get agglomerated [Fig. 4(d)].

Dynamic mechanical thermal analysis

The representative plots of storage modulus and tan delta against temperature of the S1-B20

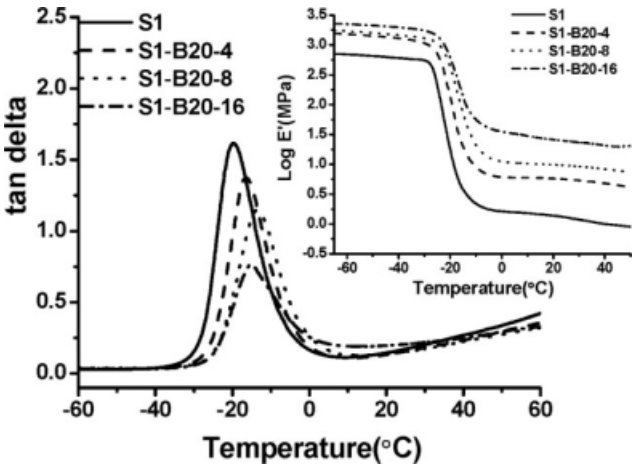

Figure 8 Log E' and tan delta vs. temperature plot of HNBR-filler nanocomposites at different loadings.

nanocomposite at different filler loadings are depicted in Figure 8. The values of T_g (glass transition temperature) and storage modulus at 25°C for neat S1 and its nanocomposites at different filler loadings are listed in Table V.

The glass transition temperature (T_g) and storage modulus of the neat rubber at 25°C are obtained as −20°C and 0.1 MPa respectively. The T_g shifts from −20°C to −15°C for S1-30B-4, −16°C for S1-B20-4, and −18°C for both S1-15A-4 and S1-A300-4. The storage modulus, on the other hand, is improved by 600% for both S1-30B-4 and S1-B20-4, 400% for S1-15A-4 and 100% for S1-A300-4. Hence, there has been a tremendous improvement in storage modulus for all the nanocomposites, as compared to the neat rubber. However, the increment is highest for S1-30B-4 and S1-B20-4. Thus, like thermal property, both B20 and 30B provide similar effects in improving the dynamic mechanical properties of the neat rubber due to the same reason as explained earlier.

Next, the effect of filler loading on the dynamic mechanical properties of rubber-clay nanocomposites has been studied using S1-B20 nanocomposites at four different filler loadings viz 4, 6, 8, and 16 phr. The plot of log E' and tan δ against temperature are represented in Figure 8. It is observed that both in the glassy as well in the rubbery region, the storage modulus increases with increase in the filler loading. The glass transition temperature shows a shift from −20°C to −13°C with filler loading up to 8 phr. No further increase in T_g value is observed at still higher loading (S1-B20-16) due to agglomeration.

Thermodynamic interpretation

The above results can be explained with the help of thermodynamics, where free energy of mixing can be calculated.

By definition,

$$\Delta G_E = \Delta H_E - T\Delta S_E \quad \text{for elastomers} \tag{1}$$

$$\Delta G_C = \Delta H_C - T\Delta S_C \quad \text{for nanofillers} \tag{2}$$

where ΔH_E, ΔH_C, ΔS_E, and ΔS_C are the enthalpy and entropy increments associated with the mixing process for the elastomer and the nanofillers respectively.

From eqs. (1) and (2), we can write, free energy change of the system during mixing is

$$\Delta G_S = \Delta G_E + \Delta G_C = (\Delta H_E + \Delta H_C) - T(\Delta S_E + \Delta S_C) = \Delta H_S - T\Delta S_S \tag{3}$$

From the expression, ΔG_S value will be negative and hence the most favorable interaction between the nanofiller and the rubber will take place, when ΔH_S is negative and ΔS_S is positive.

ΔH_S of eq. (3) has been calculated for different nanocomposites from the IR spectra (Fig. 9) using Fowkes's Equation[37] [eq. (4)] and the values are tabulated in Table VI.

$$\Delta H_S = 0.236 \times \Delta v \tag{4}$$

TABLE V
Effect of Nature of Filler and Filler Loading on Dynamic Mechanical Properties of HNBR-Filler Nanocomposites

Sl. No.	System	T_g (°C)	Storage modulus at 25°C (MPa)
1	S1	−20	0.10
2	S1-30B-4	−15	0.70
3	S1-15A-4	−18	0.50
4	S1-B20-4	−16	0.70
5	S1-A300-4	−18	0.20
6	S1-B20-6	−14	1.00
7	S1-B20-8	−13	1.20
8	S1-B20-16	−14	1.40

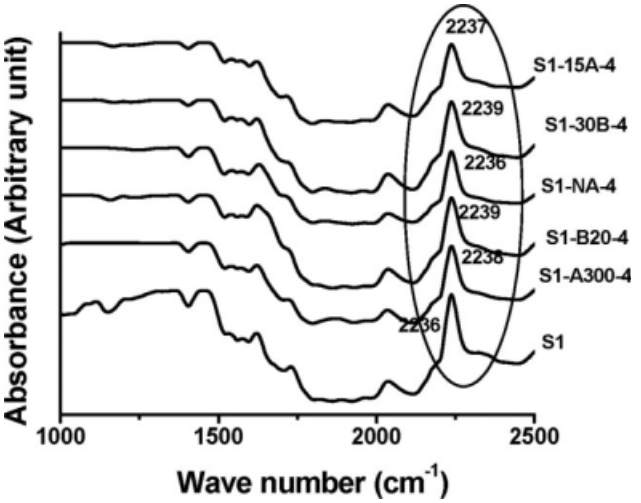

Figure 9 IR spectra of different S1-filler nanocomposites.

As depicted in Figure 9, the peak for acrylonitrile group of S1 appears at 2236 cm^{-1}. However, for the nanocomposites, this peak is shifted to 2239 cm^{-1}, 2239 cm^{-1}, 2238 cm^{-1}, 2237 cm^{-1} and 2236 cm^{-1} for S1-B20-4, S1-30B-4, S1-A300-4, S1-15A-4 and S1-NA-4 respectively (Table VI). The shift in the peak indicates the level of interaction between the polymer and the filler in line with our observation on other systems.[38] For S1-30B-4 and S1-B20-4, this shift is highest, indicating highest level of interaction. For S1-NA-4, no peak shift demonstrates poor interaction.

The thermodynamic aspects of nanocomposite formation may further be examined using the mean-field lattice-based description of polymer melt intercalation as discussed by Vaia and Giannelis.[39] An advantage of the model is the ability to analytically determine the effect on hybrid formation from various characteristics of the polymer and organically modified layered silicates. However, this model has been derived only for layered silicates. Briefly, the free energy change per interlayer volume, Δf_V, associated with polymer intercalation, has been expressed as[39]

$$\Delta f_v = \Delta e_v - T\Delta s_v \tag{5}$$

where Δe_v and Δs_v are the internal energy and entropy change per interlayer volume, respectively, given as

$$\Delta s_v = N_A K_B[\Delta s_v^{\text{chain}} + \Delta s_v^{\text{polymer}}]$$

$$= N_A K_B\left[\frac{\phi_2}{v_2}\ln(c)(\chi_s - \chi_{s0}) - \frac{\phi_1}{v_1}\left\{\frac{\pi^2}{6}\left(\frac{a_1}{h}\right)^2 + \sqrt{3}\frac{u}{\sqrt{m_1}}\frac{a_1}{h}\right\}\right] \tag{6}$$

$$\Delta e_v = \phi_1\phi_2\frac{1}{Q}\left(\frac{2}{h_0}\varepsilon_{sp,sa} + \frac{2}{r_2}\varepsilon_{ap}\right) \tag{7}$$

Δs_V is expressed as the sum of the entropy change associated with the organically-modified silicate $\Delta s_V^{\text{chain}}$, and the entropy change associated with the confinement of the polymer, $\Delta s_V^{\text{polymer}}$. h_0 and h are the initial and final gallery height after polymer intercalation, respectively. m_i, v_i, φ_i, r_i, and a_i are the number of segments per chain, the molar volume per segment, the interlayer volume fraction, the radius of the interaction surface, and the segment length of the ith interlayer species. u is a dimensionless excluded volume parameter, Q is a constant near unity, and χ_S and χ_{S0} are the fraction of interlayer volume near the surface at height h and h_0, respectively, which influence the potential chain conformations. ε_{ap} represents the pair wise interaction energy per area between the aliphatic chains and the polymer and $\varepsilon_{sp,sa} = \varepsilon_{sp} - \varepsilon_{sa}$, is the difference between the pairwise interaction energy per area between the aliphatic chain and the surface, ε_{sa}, and that between the polymer and the surface, ε_{ap}. $\chi_S(h)$ can be constructed as:

$$\chi_s(h) = \frac{a_2}{h}\cos^2\left(\frac{\pi}{2}\frac{h}{h_\infty}\right) \tag{8}$$

Values of the various parameters are listed in Table VII and the values of Δe_v and Δs_v calculated for S1-30B-4, S1-15A-4 and S1-NA-4 from eqs. (6) and (7) are listed in Table VIII.

It is a well known fact that mixing of two components is most favorable when free energy change (ΔG_S or Δf_v) of the system, is negative. From both Tables VI and VIII, it is found that ΔH_S and Δe_V for S1-30B-4 and S1-B20-4, are negative and lowest. Hence, ΔG_S or Δf_v is least for these two nanocomposites. In the case of S1-NA-4, ΔH_S and Δe_V are zero and +0.84 nm^{-1} respectively, indicating the fact that mixing of this clay in the rubber matrix is not favorable. Hence, both the approaches make similar prediction.

Vaia and Giannelis[39] in their work suggested that, during polymer intercalation from solution, the

TABLE VI
Values of ΔH_S for Different Nanocomposites

Sample name	Peak position (cm^{-1})	ΔH_S (kcal/mol)
S1	2236	–
S1-B20-4	2239	−0.708
S1-30B-4	2239	−0.708
S1-A300-4	2238	−0.472
S1-15A-4	2237	−0.236
S1-NA-4	2236	0

TABLE VII
Parameters[39] for the Nanocomposites Based on Organically Modified and Unmodified Montmorillonite Clay and HNBR, Used in Eqs. (6) and (7)

Parameters	Designation	Values
Initial gallery height (nm)[a]	h_0	
	S1-30B-4	1.98
	S1-15A-4	3.26
	S1-NA-4	1.20
Final gallery height[a] (nm)	h	
	S1-30B-4	4.8[b]
	S1-15A-4	4.3
	S1-NA-4	1.6
Tethered chain segment length (nm)	a_2	0.25
Molar volume (cm^3)	v_2	33
No. of segments[c]	m_2	9.5
HNBR statistical segment length (nm)	a_2	0.8[d]
Polymer molar volume	v_1	$3v_2$
Polymer excluded volume parameters	$\frac{u}{\sqrt{m_1}}$	0.8

[a] Obtained from XRD studies [Fig. 3(a–d)].
[b] For 30B having exfoliated morphology $h = 2h_\infty$.[39]
[c] The length of the ammonium group is approximated as half of the length of a C_2H_4 unit.[39]
[d] Ref. 40.

entropy loss of the intercalated polymer is compensated for by an entropy gain by the increased conformational freedom of the surfactant chain as the clay layer separates. They further suggested that complete layer separation depends on the establishment of very favorable polymer-organic layered silicates interaction. From Table VIII, it is found that entropy change per interlayer volume for S1-30B-4 and S1-15A-4 is +ve, while for S1-NA-4, this value is −ve. These results further prove that for S1-NA-4, the interaction between polymer and clay is not favorable. In the former approach, however, ΔS term cannot be quantitatively determined. Qualitatively, when the polymer chains enter and get trapped in the rubber matrix in the initial stage as in S1-30B-4, then the motion of the chains is restricted and as a result ΔS_E is expected to be negative. However, in the later stage, the polymer chains break the layer structure of the clay until complete exfoliation occurs and the silicates are distributed throughout the matrix (as evident from TEM and XRD results), accounting for a highly positive ΔS_C and compensating the entropy loss in the initial stage. Hence, the overall entropy change ΔS_S is expected to be positive, making ΔG_S negative. On the other hand, fibrous like particles are distributed throughout the matrix in S1-B20-4, as evident from the TEM photograph and hence ΔS_S should be positive and thus free energy change for such system is negative. In S1-A300-4, some spherical clay particles interact with rubber matrix and dispersed throughout the matrix, while some other particles form agglomeration which is clearly observed from the TEM photograph, making ΔG_S value of the system unfavorable.

The above thermodynamic phenomenon explains why improvement of mechanical and dynamic mechanical properties is best in the case of S1-30B-4. S1-A300-4 though having intermediate mechanical and dynamic mechanical properties, but its thermal property is best because of high thermal stability of A300.

CONCLUSIONS

HNBR nanocomposites have been prepared by solution mixing of HNBR with various nanofillers. Organically modified and unmodified layered silicates such as Cloisite NA, Cloisite 30B and Cloisite 15A, rod-like sepiolite and spherical nanosilica have been chosen. Significant improvement in thermal stability has been obtained for the silica-filled nanocomposite where T_{max} is improved by 16°C over the neat elastomer at 4 phr loading. This is attributed to the high thermal stability of A300 particles. These particles have a tendency to form agglomeration because of the presence of active silanol group on its surface (as observed from the TEM photograph) for which the mechanical properties drop. From the x-ray diffractogram and the TEM photograph, it is found that 30B has undergone full exfoliation

TABLE VIII
Values of Δe_v and Δs_v for Different Nanocomposites

Sample name	Δev (nm^{-1})	Δs_v (J K^{-1} $mol^{-1}m^{-3}$) × 10^{-3}
S1-30B-4	−0.20	+1.58
S1-15A-4	−0.05	+0.77
S1-NA-4	+0.84	−20

within the bulk of the matrix, and thus provides highest tensile strength, excellent storage modulus and very good thermal stability. Sepiolite, because of its fibrous nature, high aspect ratio and uniform dispersion (as observed from TEM photograph) gives rise to excellent improvement in modulus at 100% elongation and storage modulus and also provides very good thermal stability to the matrix. It is further observed from the XRD and TEM photograph, the nanocomposite based on 15A clay exhibit intercalated structure which is responsible for intermediate thermal, mechanical and dynamic mechanical property to the matrix. Unmodified NA particles, on the other hand, form agglomeration on addition to the rubber matrix, which is clearly observed from the XRD and the TEM photograph, and thus NA has the least effect on the thermal and mechanical properties of the elastomer. With the increase in filler loading, both thermal as well as mechanical properties of HNBR-filler nanocomposites have increased up to 8 phr loading, beyond which these show a decreasing trend because of agglomeration, as observed in transmission electron micrographs. The results are further explained with the help of thermodynamics. For example, the enthalpy change and the internal energy change per interlayer volume are negative and hence lowest for S1-30B-4 and S1-B20-4 and hence favorable. The entropy change per interlayer volume is negative for S1-NA-4 and explains the poor dispersion of unmodified montmorillonite.

The authors are indebted to LANXESS, Germany for funding the project at IIT Kharagpur.

References

1. Stephens, H. L.; Bhowmick, A. K. Handbook of Elastomer, 2nd ed.; Marcel Dekker: New York, 2000.
2. Bhattacharjee, S.; Bhowmick, A. K.; Avasthi, B. N. J. Appl Polym Sci 1990, 41, 1357.
3. Bhattacharjee, S.; Bhowmick, A. K.; Avasthi, B. N. J. Polym Sci Part-A: Polym Chem 1992, 30, 471.
4. Shach, D.; Fytas, G.; Vlassopolelos, D. Langmuir 2005, 21, 19.
5. Jordan, J. M. J Phys Colloid Chem 1950, 53, 245.
6. Joley, S. Chem Mater 2002, 14, 4202.
7. Tarapow, J. A.; Bernai, C. R.; Alvarez, V. A. J Appl Polym Sci 2009, 111, 768.
8. Maiti, M.; Bhattacharya, M.; Bhowmick, A. K. RCT 2008, 81, 384.
9. Koh, H. C.; Park, J. S.; Jeong, M. A.; Hwang, H. Y.; Hong, Y. T.; Ha, S. Y.; Nam, S. Y. Desalination 2008, 233, 201.
10. Kojima, U. A.; Okada, Y.; Kamigaito, A. J. Mater Res 1993, 8, 1185.
11. Liu, C. G.; Chen, S.; Qiz, S. Macromol Chem Phys 2001, 202, 1189.
12. Li, X.; Kang, T. K.; Cho, W. J.; Lee, J. K.; Ha, C. S. Macromol Rapid Commun 2001, 22, 1306.
13. Messermith, P. B.; Giannelis, E. P. Chem Mater 1994, 6, 1719.
14. Burnside, S. D.; Giannelis, E. P. Chem Mater 1995, 7, 1597.
15. Sadhu., S.; Bhowmick, A. K. J Polym Sci Part B: Polym Phy 2004, 42, 1573.
16. Lan, T.; Pinnavaia, J. Chem Mater 1999, 6, 2216.
17. Shen, Z.; Simon, G. P.; Cheng, Y. B. Polymer 2002, 43, 4251.
18. Choudalakis, G.; Gotsis, A. D. Europ Polym J 2009, 45, 967.
19. Kojima, Y.; Usuki, A.; Kawasumi, M.; Okada, A.; Kurauchi, T.; Kamigaito, O.; Kaji, K. J. Polym Sci Part B: Polym Phys 1995, 33, 1039.
20. Cho, J. W.; Paul, D. R. Polymer 2001, 42, 1083.
21. Hasegawan, N.; Okamoto, H.; Kato, M.; Usuki, A. J Appl Polym Sci 2000, 78, 1918.
22. Rong, J.; Jing, Z.; Li, H.; Sheng, M. Macromol Rapid Commun 2001, 22, 329.
23. Fu, X.; Qutubuddin, S. Polymer 2001, 42, 807.
24. Chen, G.; Liu, S.; Zhang, S.; Qi, Z. Macromol Rapid Commun 2000, 21, 746.
25. Wang, M. S.; Pinnavaia, T. J. Chem Mater 1998, 10, 1820.
26. Lan, T.; Kaviratna, P. D.; Pinnavaia, T. J. Chem Mater 1995, 7, 2144.
27. Chang, Y. C.; Yang, Y.; Ryu, S.; Nah, C. Polym Int 2002, 51, 319.
28. Bokobza, L.; Burr, A.; Garnaud, G.; Perrin, M. Y.; Pagnotta, S. Polym Int 2004, 53, 1060.
29. Maji, P. K.; Bhowmick, A. K. J Polym Science, Part A: Polym Chem 2009, 47, 731.
30. Ganguly, A.; Bhowmick, A. K.; Li, Y. Macromolecules 2008, 41, 6246.
31. Rong, J.; Sheng, M.; Li, H. Polym Compos 2002, 23, 658.
32. Bandyopadhyay, A.; Bhowmick, A. K. J. Polym Eng 2006, 25, 821.
33. Bandyopadhyay, A.; Bhowmick, A. K. Plastic Rubber Compos 2006, 35, 210.
34. Choudhury, A.; Ong, C.; Bhowmick, A. K. Polymer 2009, 50, 201.
35. Bhowmick, A. K.; Rampalli, S.; Gallagher, K.; Mclntyre, D. J Appl Polym Sci 1987, 33, 1125.
36. Gu, A.; Liang, G. Polym Degrad Stab 2003, 80, 383.
37. Fowkes, F. M.; Tischler, D. O.; Wolfe, J. A.; Lannigan, L. A.; Ademu-John, C. M.; Halliwell, M. J. J Polym Sci Part A: Polym Chem 1984, 22, 547.
38. Maiti, M.; Bhowmick, A. K. Polym Sci Part B: Polym Phy 2006, 44, 162.
39. Vaia, R. A.; Giannelis, E. P. Macromolecules 1997, 30, 7990.
40. Bhowmick, A. K.; Chiba, T.; Inoue, T. J Appl Polym Sci 50, 2055.